Towards optimization of experimental parameters for studying Li-O_2 battery discharge products in TEM using in situ EELS

Basak, Shibabrata; Jansen, Jacob; Kabiri, Yoones; Zandbergen, Henny W.

DOI
10.1016/j.ultramic.2018.03.005

Publication date
2018

Document Version
Final published version

Published in
Ultramicroscopy

Ultramicroscopy 188 (2018) 52–58

Contents lists available at ScienceDirect

Ultramicroscopy

journal homepage: www.elsevier.com/locate/ultramic

Towards optimization of experimental parameters for studying Li-O_2 battery discharge products in TEM using *in situ* EELS

Shibabrata Basak*, Jacob Jansen, Yoones Kabiri, Henny W. Zandbergen

Kavli Institute of Nanoscience, Delft University of Technology, Lorentzweg 1, Delft 2628CJ, The Netherlands

ARTICLE INFO

Article history:
Received 6 November 2017
Revised 13 February 2018
Accepted 2 March 2018
Available online 6 March 2018

Keywords:
Li–O_2 battery
TEM study
e-beam damage
Air exposure
Graphene cell
In-situ EELS

ABSTRACT

The key to understanding the performance of Li–O_2 batteries is to study the chemical and structural properties of their discharge product(s) at the nanometer scale. Using TEM for this purpose poses challenges due to the sensitivity of samples to air and electron beams. This paper describes our use of *in situ* EELS to evaluate experimental procedures to reduce electron-beam degradation and presents methods to deal with air sensitivity. Our results show that Li_2O_2 decomposition is dependent on the total dose and is approximately 4–5 times more pronounced at 80 than at 200 kV. We also demonstrate the benefits of using low-dose-rate STEM. We show further that a "graphene cell", which encapsulates the sample within graphene sheets, can protect the sample against air and e-beam damage.

1. Introduction

Lithium–air or, more accurately, Li–O_2 battery with a high theoretical specific energy has attracted a lot of attention recently [25,15,19]. As the name suggests, the operating principle of Li–O_2 battery is based on the interaction between lithium (Li) and oxygen (O_2). In a non-aqueous Li–O_2 battery, oxidation occurs at the anode ($Li \rightarrow Li^+ + e^-$) and lithium ions ($Li^+$) are transported via the electrolyte towards the porous cathode support, where they react with the incoming oxygen and electrons, flowing through an external circuit, to form a reversible discharge product of lithium peroxide (Li_2O_2) [19,4]. During charging, Li_2O_2 decomposes to Li^+ and O_2. Worldwide research in the past five years has given us a better understanding of the complex chemistry involved in this process [23,21,1]. However, high overpotential during charging, poor capacity retention and low cycle life are still the main obstacles to developing applications of Li-O_2 battery technology [12,7].

It has been reported that the reversibility and charge overpotential of Li–O_2 batteries depend strongly on the morphology of Li_2O_2. Small peroxide particles cause a lower charge overpotential than large ones do [16,17]. It has been also reported that large current densities (>200 μA/cm^{-2}) lead to a quasi-amorphous thin-film discharge product. The morphology of the discharge product also depends on the type of carbon support and electrolytes used in the battery [14].

In addition to the desired Li_2O_2, several undesired discharge products are also formed. Depending on the electrolyte and current density, it has been reported that significant amounts of irreversible Li_2O can form [7]. Moreover, several carbonate-based products including lithium carbonates produced by decomposed electrolytes, especially in carbonate-based electrolytes, have been reported [13]. Ether-based electrolytes, which are less prone than carbonate-based electrolytes to superoxide attack, are a better choice for Li-O_2 battery because their main discharge product is Li_2O_2 [3]. Carbon, the material most commonly used as a porous cathode support, can form carbonates caused by side reactions with the electrolyte [20]. Recently, several carbon-free support cathodes such as nano-porous gold, indium–tin oxide and titanium nitride have been used to avoid parasitic reactions involving carbon and electrolyte and/or Li_2O_2, and hence to reduce the charge overpotential and improve the cycling performance of Li-O_2 batteries [22,18,5]. Furthermore, catalyst nanoparticles dispersed on a porous cathode support have been used to improve the (dis)charge overpotential and prolong the cycle life [18,5]. It has been speculated that the catalyst particles control the growth of Li_2O_2 facets and facilitate the growth of kinetically active facets, thus improving the reaction kinetics. Nevertheless, the working mechanisms of these catalysts are far from understood.

The chemical properties of Li-O_2 batteries could be understood in detail by analyzing the discharge product with respect to different carbon and non-carbon cathode supports, binders and elec-

* Corresponding author.
E-mail addresses: s.basak@tudelft.nl (S. Basak), j.jansen@tudelft.nl (J. Jansen), y.kabiri@tudelft.nl (Y. Kabiri), h.w.zandbergen@tudelft.nl (H.W. Zandbergen).

https://doi.org/10.1016/j.ultramic.2018.03.005
0304-3991/

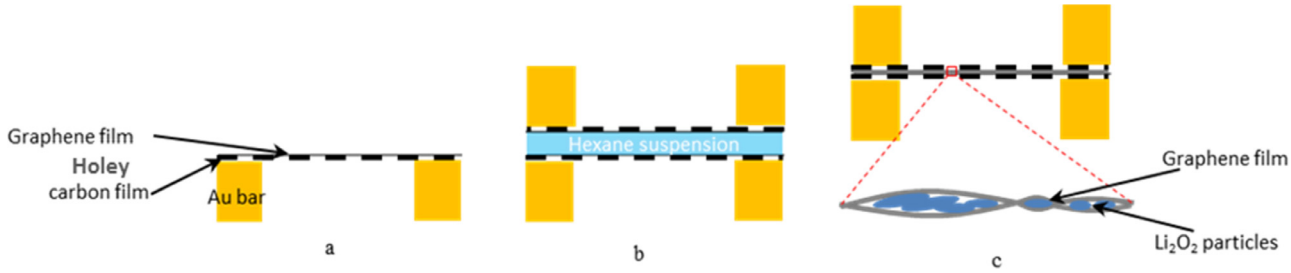

Fig. 1. Schematic illustration of graphene cell preparation. The process is performed inside an argon glove box. (a) Holey-carbon TEM grid with graphene. (b) Li_2O_2 suspension in hexane is dripped onto the grid. Before the hexane has evaporated, a second grid is placed on top of it. (c) As the hexane evaporates, the graphene films adhere to each other, thus encapsulating Li_2O_2 particles to form a "graphene cell".

trolytes. Furthermore, structural and chemical studies of the discharge product at the nanometer scale are needed to find probable crystallographic and/or compositional variations between the discharge products grown on catalyst particles and those grown on other areas of the cathode. This will enhance our ability to develop better catalyst/grain refiner nanoparticles.

Transmission electron microcopy (TEM) studies of the discharge products allow crystallographic and compositional analysis at the sub-nanometer scale. However, the air and electron-beam sensitivity of the discharge products makes it difficult to retain the pristine condition of the sample throughout TEM measurements, which can render the results unreliable. In this work, we evaluate ways to avoid air and e-beam degradation by using *in situ* EELS to analyze discharge products in their pristine form.

2. Experimental details

We used Li_2O_2, Li_2O and Li_2CO_3 samples obtained from Sigma Aldrich to find the best conditions under which air and e-beam degradation can be prevented. After crushing the sample, we prepared a suspension in anhydrous hexane, which we dripped onto TEM grids. All sample preparations are performed inside a glove box filled with argon and with O_2 and H_2O levels of < 1 ppm. To prevent exposure of the sample to air, TEM grids are loaded into a custom-made vacuum transfer TEM holder inside the glove box. For experiments with the "graphene cells" described below, a standard TEM holder is used.

2.1. Graphene cell preparation

We prepared "graphene cells" by encapsulating Li_2O_2 particles between graphene sheets as follows. First, multilayer (3–4 layers) graphene films are transferred onto standard holey-carbon TEM grids, following the procedure described in reference [6]. Briefly, standard Au Quantifoil grids (with holey-carbon film) are placed on top of CVD-grown graphene on copper foil, onto which drops of isopropanol are applied. As the isopropanol evaporates, the holey-carbon film of the grid adheres to the graphene. The copper foil is then etched away with a $FeCl_3$ solution, and the graphene-coated grids are rinsed several times with deionized water. Finally, the grids are removed from the water and left on filter paper to dry in ambient temperature.

Two such grids form the scaffold of a graphene cell as follows. First, drops of the hexane suspension containing the Li_2O_2 particles are applied to the graphene sides of the grids. Then, before the solution has completely evaporated, one graphene grid is immediately placed face down on top of the other. As the hexane evaporates, the graphene sheets adhere to each other, thereby encapsulating the Li_2O_2 particles. We prepared the graphene cells inside an argon glove box as schematically shown in Fig. 1.

2.2. TEM investigation and Li_2O_2 fraction calculation

TEM measurements are performed in a FEI Tecnai microscope equipped with a Gatan EEL spectrometer and operated at 80 and 200 kV. EEL spectra are recorded in diffraction mode with a resolution of 0.7 eV, determined from the full width at half maxima of the zero-loss peak. Li–K and O–K edges are recorded at acquisition times of 0.1 and 5 s, respectively.

Under e-beam exposure, Li_2O_2 gradually decomposes to Li_2O, meaning that the proportion of Li_2O_2 in the sample decreases with increasing Li_2O. To determine which experimental conditions will retain Li_2O_2 in pristine condition the longest during TEM analysis, we acquired time-evolved EELS series for different experimental conditions.

The fraction of Li_2O_2 at each instant of an EEL spectra series is calculated as follows. Background-subtracted pristine Li_2O_2, indicated by the absence of a peak at 533 eV, and 50% decomposed Li_2O_2, indicated by peaks of equal intensity at 530 and 533 eV, are designated as two reference spectra. To determine the proportion fraction of Li_2O_2 in a spectrum, the background is subtracted from the spectrum and a least-squares fit is used to calculate the two scale factors to be applied to the reference patterns such that their sum best matches the spectrum under consideration. A simple computer program is written to automate the spectra analysis. Although we took extreme care to choose areas with similar particles for all the different series, thickness variations between the areas cannot be eliminated. And since the thickness variation in the sample may affect the EELS edge profile, which in turn would affect our ability to quantify the fraction of Li_2O_2, we assigned the reference spectra from the corresponding series. If the first spectrum of the series already contained a peak at 533 eV, a spectrum from another area with no peak at 533 eV is used as the first reference. Note that such reference spectra can lead to a less reliable analysis.

3. Results

We studied the effect of air and e-beam exposure on Li_2O_2, Li_2O and Li_2CO_3 using electron energy loss spectroscopy (EELS). EELS is a very powerful technique that can provide detailed chemical information about the sample under TEM investigation [8]. Background-subtracted Li–K and O–K edge EEL spectra acquired from Li_2O_2, Li_2O and Li_2CO_3 are shown in Fig. 2(a) and (b), respectively. These EEL spectra agree well with previously reported XAS spectra [24]. The unambiguous differences between the spectra of Li_2O_2, Li_2O and Li_2CO_3 are due to differences in the local Li and O environments in these compounds. These spectra can be used as reference spectra to verify the chemical compositions of the Li–O_2 battery discharge product. One of the predominant differences in the EEL spectra is the O–K edge position for Li_2O_2 (at 530 eV) and Li_2O (at 533 eV). Therefore, O–K edge is monitored for further studies.

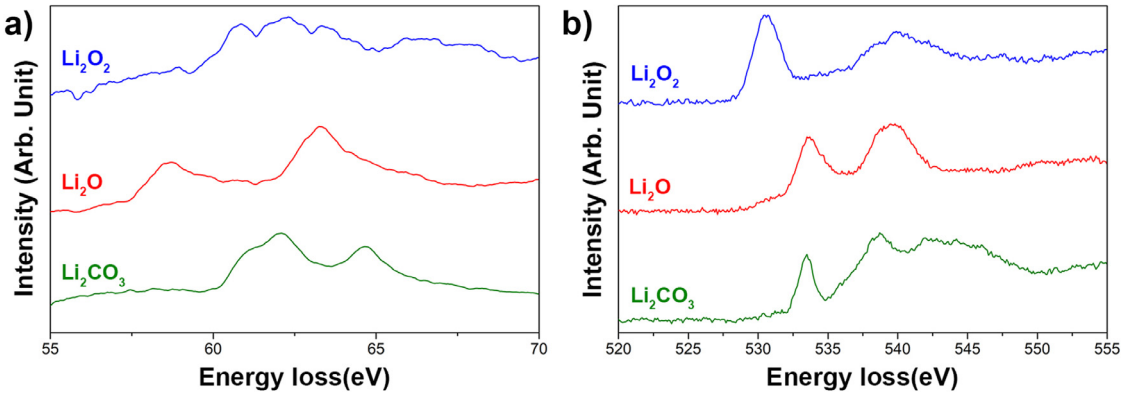

Fig. 2. Li_2O_2, Li_2O and Li_2CO_3 EEL spectra (a) Li–K edge and (b) O–K edge.

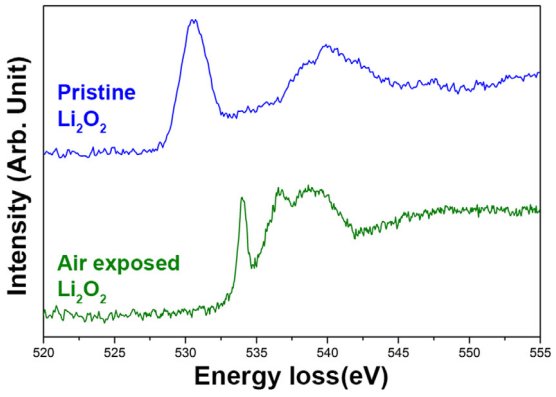

Fig. 3. Effect of air exposure on Li_2O_2 is shown by the O–K edge EEL spectra.

The air-sensitive nature of Li_2O_2 is shown in Fig. 3. The EEL spectrum acquired from Li_2O_2 exposed to air for one hour in ambient atmosphere is quite different from that of the Li_2O_2 not exposed to air, which was obtained using a homemade TEM holder with a vacuum transfer stage.

Electron beam irradiation in a TEM can change the pristine nature of Li_2O_2 and Li_2CO_3 samples. Fig. 4(a) shows the typical evolution of O–K edge Li_2O_2 EEL spectra under 200-kV electron beam exposure. Increasing e-beam exposure reduced the intensity of the peak at 530 eV, whereas a further created a new peak at 533 eV. The simultaneous reduction of the peak at 530 eV and the increase at 533 eV with increasing e-beam exposure reveals that e-beam irradiation transformed Li_2O_2 into Li_2O. The detailed evolution of the EEL spectra during the transformation can be viewed in Movie S-1. It is evident in Fig. 4(b) and (c) that e-beam irradiation transformed the single crystalline Li_2O_2 particles into polycrystalline Li_2O. The complete evolution of Li_2O_2 particles under e-beam irradiation can be viewed in Movies S-2a and S-2b. It is apparent that this transformation did not proceed via core-shell growth, where Li_2O would be is the newly formed shell. Like Li_2O_2, Li_2CO_3 is transformed under e-beam irradiation to Li_2O, as can be concluded from Fig. 4(d).

For a reliable chemical and structural analysis of the discharge product, it is essential to retain the sample in pristine condition throughout the measurements. Thus, the transformation of discharge product due to air exposure and e-beam irradiation must to be eliminated. Using a vacuum transfer TEM holder eliminates air exposure of the TEM sample during the transfer process. Therefore, air contact to the sample can be completely avoided if the TEM sample is prepared and loaded into a vacuum transfer TEM holder in a glove box. Although it is not possible to eliminate e-beam irradiation damage completely, suitable imaging conditions can delay the onset of Li_2O_2 decomposition long enough to acquire information from the pristine sample. Thus, the main goal of the research reported in this paper is to determine the optimal imaging parameters that delay the onset of Li_2O_2 decomposition, which we achieved using *in situ* EELS as will be discussed in the following sections.

3.1. TEM acceleration voltage

It is well known that acceleration voltage plays a significant role in determining e-beam damage [11,9]. To check the effect of acceleration voltage on the decomposition rate of Li_2O_2, EELS measurements are carried out at 80 and 200 kV with the same electron dose rate of 8900 e/nm^{2}s. Fig. 5 compares the O–K edge EEL spectra acquired at 80 and 200 kV from a fresh sample area not subjected to prior e-beam exposure. Note that during the acquisition time (5 s) of an EEL spectrum, the fresh areas are exposed to e-beam irradiation. The samples are exposed to additional irradiation for approximately another 5 s, which is the time required to set up the microscope for the EEL spectrum acquisition. Therefore, for the EEL spectra under consideration, the fresh areas are actually exposed to some 10 s of e-beam irradiation. The EELS spectrum acquired at 80 kV shows peaks at 530 and 533 eV. This indicates that a significant fraction of the Li_2O_2 particles are transformed into Li_2O (Li_2O_2 fraction in the sample is ~70%). The EEL spectrum acquired at 200 kV with the same electron dose shows no detectable peak at 533 eV, meaning that no decomposition occurred during exposure. This indicates that e-beam irradiation damage for Li_2O_2 is faster at 80 than at 200 kV. Moreover, as can be inferred from Fig. 6(a), it takes 4–5 times longer for the electron irradiation at 200 than at 80 kV to decompose similar amounts of Li_2O_2 (Li_2O_2 fraction in the sample is ~70%). Thus, to retain the pristine nature of Li_2O_2 for longer periods, imaging is better at 200 than at 80 kV.

3.2. Electron dose rate

The Li_2O_2-to-Li_2O transformation also occurs at 200 kV. Fig. 6(a) shows for an e-beam dose rate of 8900 e/nm^{2}s how Li_2O_2 fraction in the sample is reduced. To demonstrate this process, consecutive EEL spectra are acquired from the same area of Li_2O_2 sample within 10 s of e-beam exposure, and theLi_2O_2 fraction in the sample is then determined from each spectrum. Please refer to the experimental section for details. The graph shows that, for a dose rate of 8900 e/nm^{2}s, the onset of Li_2O_2 decomposition began after 20 s of e-beam exposure. Thus, Li_2O_2 samples remain in pristine condition for the first 20 s of e-beam exposure. Further irradiation reduced the proportion of Li_2O_2, and 50% of the Li_2O_2 had decomposed within 160 s.

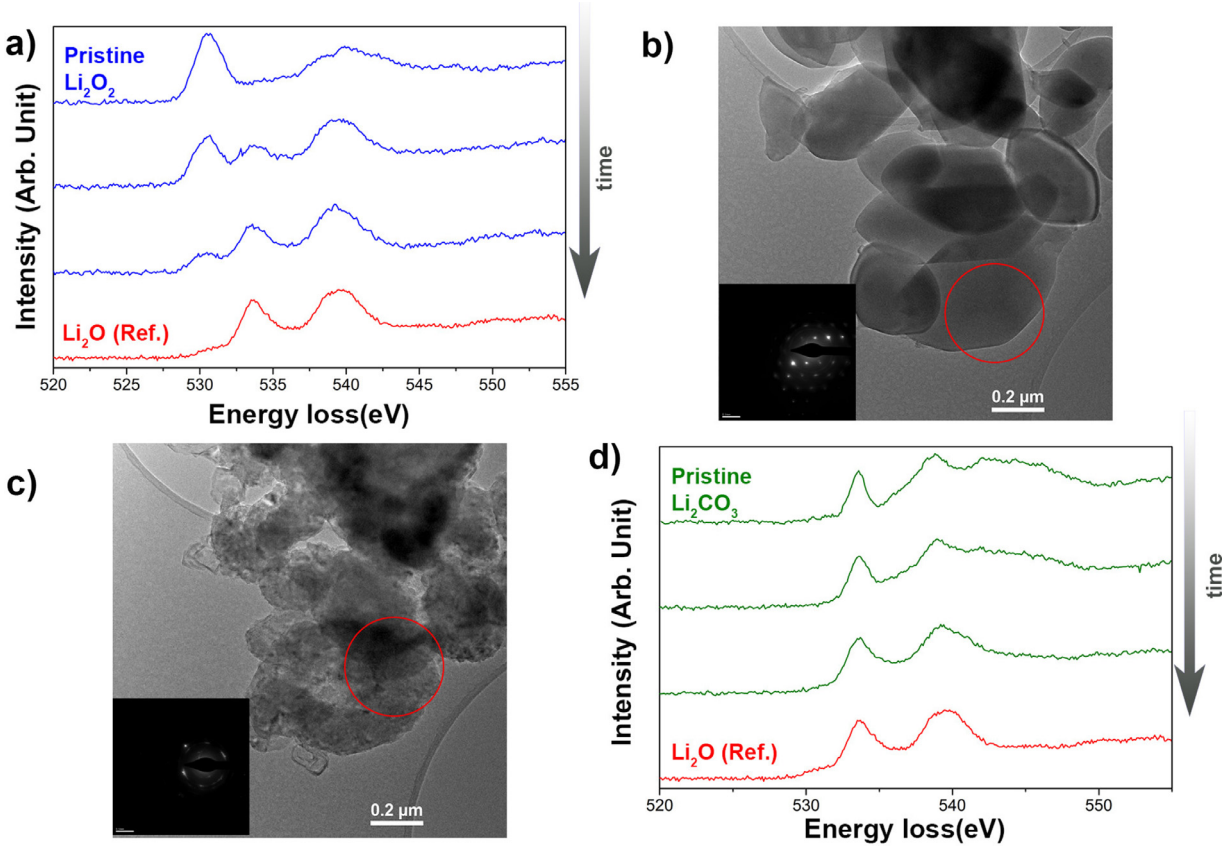

Fig. 4. (a) Effect of e-beam irradiation on Li_2O_2 revealed by the O–K edge EEL spectra. Li_2O EEL spectrum is given as a reference. All O–K edge EEL spectra are acquired at 200 kV with an acquisition time of 5 s using a vacuum transfer holder. Owing to e-beam exposure, single crystalline Li_2O_2 particles (b) are transformed into polycrystalline Li_2O (c). (d) Effect of electron beam irradiation on Li_2CO_3.

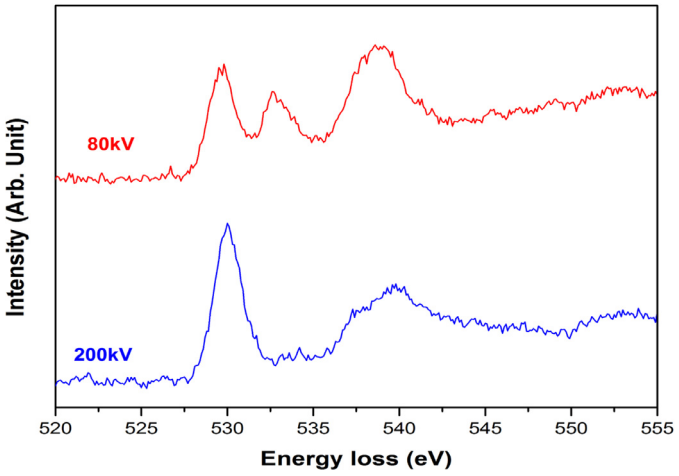

Fig. 5. Comparison of the e-beam irradiation effect on Li_2O_2 at different acceleration voltages. Both spectra are recorded from a fresh spot of the sample with electron dose rate of 8900 e/nm^{2}s.

To determine the dependence of decomposition onset on the dose rate, we repeated our experiment with different dose rates. Fig. 6(b) compares the time required to initiate Li_2O formation for 1900, 8900 and 38,000 e/nm^{2}s. For a dose rate of 1900 e/nm^{2}s, the onset of decomposition is delayed for 60 s, whereas for a dose rate of 38,000 e/nm^{2}s and above, no onset of decomposition is observed (first acquired EEL spectrum shows a presence of Li_2O). Thus, it can be concluded that the decomposition onset can be delayed by using a lower dose rate. The total dose required to initiate Li_2O formation for dose rates of 1900 and 8900 e/nm^{2}s are $\sim 1.14 \times 10^5$ and 1.78×10^5 e/nm^2, respectively. The dependence of the decomposition on the total electron dose is addressed later in the paper. The typical decomposition trends of Li_2O_2 at different electron dose rates are shown in Fig. S-3.

To verify these decomposition trends, we repeated the experiment for each dose rate. Variations in decomposition time are found between different measurements at the same dose rates, see Fig. S-4(a). These differences can be attributed to the different thicknesses of the samples, where thin samples are prone to damage sooner, as reported by Egerton [11]. Slow transformations of thick Li_2O_2 samples are observed (not included here). The times required for 50% Li_2O_2 decomposition from various experiments are shown in Fig. S-4(b).

3.3. Graphene cell

It is predicted in the literature that conductive coating could reduce e-beam irradiation damage in insulating samples [11]. With this in mind, we used a graphene cell, which encapsulate the sample with conductive graphene sheets. A schematic description of graphene cell preparation is shown in Fig. 1. To determine whether a graphene cell can reduce the e-beam decomposition of Li_2O_2, we acquired several EEL spectra series. Fig. 7(a) shows a typical decomposition of Li_2O_2 in a graphene cell for a dose rate of 8900 e/nm^{2}s. Compared to a standard grid sample, the graphene cells delayed the onset of Li_2O_2 decomposition: Li_2O_2 in a graphene cell withstood four times the e-beam exposure than a standard grid sample. The variation in the effectiveness of graphene cells against e-beam decomposition is described further on in this paper. With increasing e-beam exposure, Li_2O_2

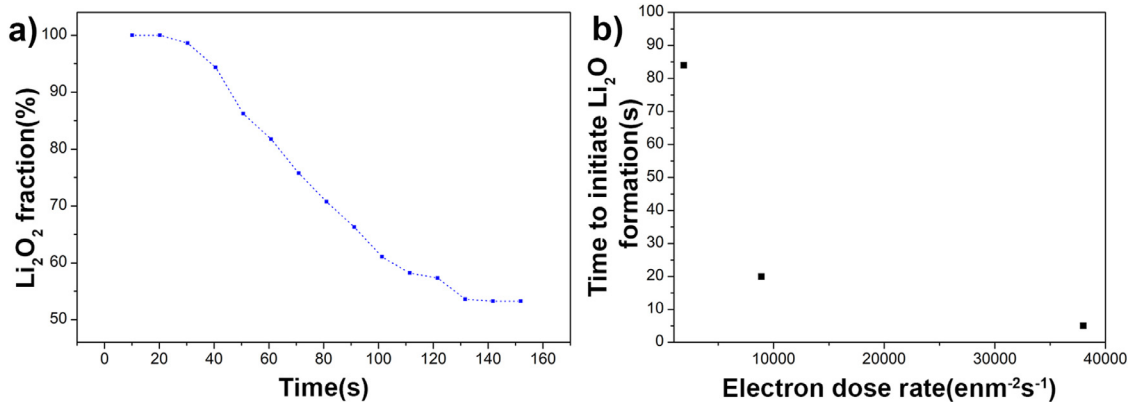

Fig. 6. (a) Typical decomposition trend of Li_2O_2 with dose rate of 8900 e/nm^{2}s. (b) Effect of electron dose rate to initiate Li_2O formation. All data are for 200 kV irradiation.

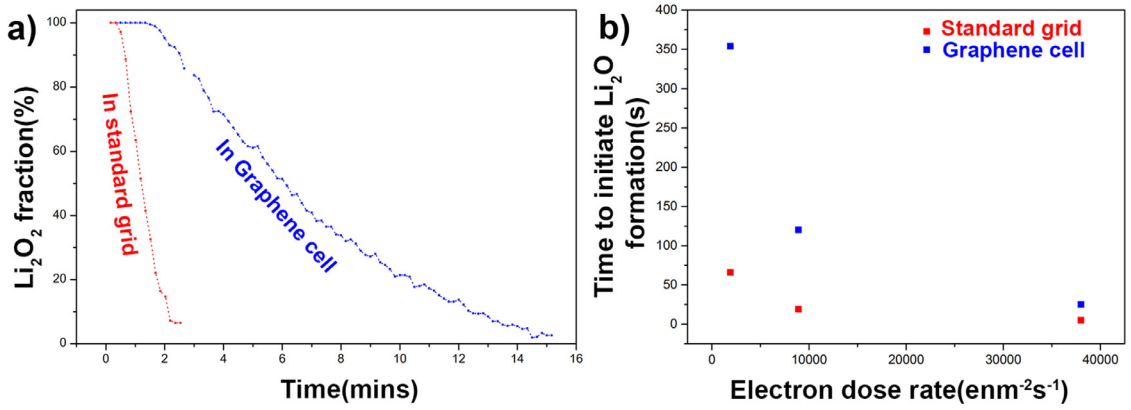

Fig. 7. Effectiveness of a graphene cell in delaying the formation of Li_2O. (a) A typical decomposition trend of Li_2O_2 with a dose rate of 8900 e/nm^{2}s. (b) Effect of electron dose on Li_2O formation onset. All data are for 200 kV irradiation. Average values from the standard grid are given as a reference.

in a graphene cell began to decompose and, within 15 min of e-beam exposure, 50% of the Li_2O_2 had decomposed into Li_2O. As in the standard grid, the onset of Li_2O_2 transformation is further delayed in a graphene cell when the electron dose rate is reduced to 1900 e/nm^{2}s. In this case, no detectable Li_2O_2 decomposition had occurred for the first 350 s of e-beam exposure, which is four times higher than that for an electron dose rate of 8900 e/nm^{2}s in a graphene cell and approximately six times more than that with a standard grid at the same electron dose rate of 1900 e/nm^{2}s. The effectiveness of a graphene cell in delaying the onset of decomposition is also observed for higher dose rates. For a dose rate of 38,000 e/nm^{2}s, a graphene cell delays Li_2O_2 decomposition for 25 s, compared to a standard grid, in which an average of 20% of Li_2O_2 decomposed after 10 s of e-beam exposure. When the e-beam dose rate is increased to 225,000 e/nm^{2}s, no decomposition was observed in samples encapsulated in a graphene cell. Fig. 7(b) compares the time required to initiate Li_2O_2 decomposition in graphene cells and standard grid samples at different dose rates. The total doses required to initiate Li_2O formation in a graphene cell for dose rates of 1900, 8900 and 38,000 e/nm^{2}s are $\sim 6.65 \times 10^5$, 10.68×10^5 and 9.5×10^5 e/nm^2, respectively.

For samples encapsulated in a graphene cell, the oxygen released during the Li_2O_2-to-L_2O transformation would be trapped within the graphene pocket, thus creating an oxygen-rich environment. One might predict that this oxygen-rich environment delays the Li_2O_2-to-Li_2O transformation. However, we used an electron beam to drilled holes in the graphene cell close to the sample area to allow oxygen release, but observed no significant difference in the Li_2O_2 decomposition behaviour. Therefore, the oxygen-rich environment is at least not the main reason for the delayed Li_2O_2 decomposition.

To determine whether the graphene cell is consistently effective throughout the grid area, we acquired several sets of EEL spectra from different areas of the graphene cell. Fig. S-5 shows the time required for a 50% Li_2O_2 decomposition at different dose rates. Clearly, although the graphene cell shows better performance in general than the standard grid in terms of lowering the decomposition rates, but the performance of the graphene cell is not consistent everywhere. The trends of decomposition in a graphene cell at different dose rates are shown in Fig. S-6. Average decomposition curves from standard grids are shown for easy comparison. We attribute the large variation in e-beam-induced decomposition to differences in the encapsulation of Li_2O_2 by the graphene sheets. As thickness variations of the samples also led to variations, is it difficult to uncouple the performance of the graphene cell in various areas of the grid.

Apart from delaying Li_2O_2 decomposition, the graphene cell also protects Li_2O_2 from degradation due to air exposure. EEL spectra acquired from Li_2O_2 in graphene cells exposed to air are quite similar to those in non-exposed samples. This indicates that Li_2O_2 within a graphene cell can be retained in pristine condition, even if the cell is exposed to air. Therefore, a graphene cell acts as a capsule for air-sensitive discharge products. Fig. S-7 compares non-air-exposed Li_2O_2 O–K edge spectra with air-exposed samples in a standard grid and a graphene cell.

3.4. STEM mode

In scanning-TEM (STEM) mode, a focused probe is scanned over the sample residing for only a short time (generally a few μs, depending on dwell time) over the same spot. To check whether this kind of irradiation could increase the onset of Li_2O_2 de-

composition, we exposed the sample undergoing STEM scanning to different electron dose rates. In STEM, the dose rate can be changed in two ways: changing the beam dwell time or changing the pixel size by changing the magnification. For a dose rate of less than 100 e/nm^{2}s, we found that Li_2O_2 can withstand 30 min of STEM scanning without appreciable decomposition. Therefore, STEM mode is ideal for studying the morphology of the discharge product while retaining the pristine nature of the sample.

However, we observed faster Li_2O_2 decomposition with increasing dose rate. For example, at a dose rate of 100 e/nm^{2}s, Li_2O_2 under STEM scanning remains in pristine condition for 30 min, whereas for a dose rate of 28,000 e/nm^{2}s at a magnification of 160 kX and a dwell time of 50 µs, 50% of the Li_2O_2 decomposed within 30 s. Details about the parameters used during our STEM investigations are listed in Table S-8.

4. Discussion

As the reaction products of degradation caused by exposure to air or e-beam irradiation are quite similar to some of the discharge products in a Li–O_2 battery, it is essential to keep the sample in pristine condition until and during TEM analysis Degradation due to air exposure during sample transfer to the TEM can be avoided by using a vacuum transfer TEM holder or a graphene cell. In both cases, Li_2O_2 is kept in pristine condition during insertion of the sample into the TEM (Figure S-7). For the air exposure test, the TEM sample is kept at ambient atmosphere for 1 h. Therefore the changes in EEL spectra are due to air exposure of 1 h. We chose this duration of air exposure to show the effect prominently. It should be pointed out that the EEL spectrum acquired after air exposure for 2 min showed no significant difference from the non-air-exposed sample (not shown here). However, a few-nanometer-thick Li_2O_2 layer, typically formed during the fast discharge, is likely to be transformed much faster in contact with air than the sample under study. Therefore, to ensure that the sample is kept in pristine condition for TEM investigations, air exposure should be avoided entirely.

Although it is not possible to prevent e-beam damage completely, our results show that the pristine condition of Li_2O_2 can be preserved longer against e-beam irradiation by using (a) a relatively high acceleration voltage, (b) a lower electron dose rate, (c) a graphene cell and (d) STEM mode. It is observed that, at 200 kV, Li_2O_2 can sustain an electron dose that is 4–5 times higher than at 80 kV. Moreover, Li_2O_2 encapsulated in a graphene cell can sustain an electron dose that is approximately 4 times higher than Li_2O_2 in a normal TEM grid before it begins to decompose. Keeping the sample at low temperatures using a cryo-transfer holder can also help to preserve the sample in its native state; a detailed study of this parameter is the subject of further research.

Decomposition of Li_2O_2 to Li_2O occurs also if Li_2O_2 is heated. It has been reported that Li_2O_2 decomposition proceeds via Li_2O_2–Li_2O solid solution formation until 50% of the Li_2O_2 has decomposed [26,27]. However, our EELS study showed that, with increasing e-beam exposure, the peak around 530 eV became weaker and simultaneously a new peak at approximately 533 eV appeared and increased (Movie S-1). The presence of two distinct peaks at 530 and 533 eV, which are representative of Li_2O_2 and Li_2O, respectively, throughout the Li_2O_2-to-Li_2O transformation indicate that no solid solution is formed during e-beam decomposition. Furthermore, the electron diffraction Movie S-2b shows that there is no epitaxial relation between Li_2O and Li_2O_2.

For insulating materials in TEM, the knockout displacement cross section is considerably lower than that of ionization damage. Therefore, although knockout damages do occur in insulating specimens, ionization damage remains the predominant form of damage [10]. As the inelastic scattering cross section varies inversely

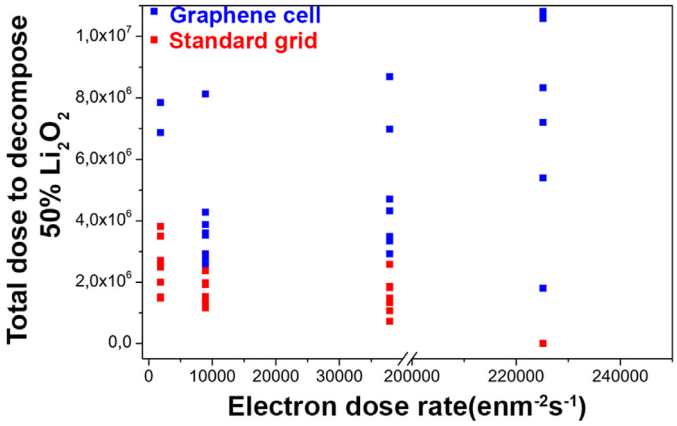

Fig. 8. Comparison between the total dose required to decompose 50% of Li_2O_2 at different dose rates in a standard grid and a graphene cell at 200 kV.

to the acceleration voltage, Li_2O_2 decomposes faster at 80 than at 200 kV.

Our experiments show that a "graphene cell" can delay Li_2O_2 decomposition as depicted in Fig. 7(b). Zan et al. and Algara-Siller et al. have demonstrated the damage reduction capability of graphene by encapsulating MoS_2 between graphene sheets [2,28]. One can argue that the configuration in our sample, unlike the almost two-dimensional graphene–MoS_2–graphene sandwich, is quite different: the Li_2O_2 particles are tens of nanometers thick and are only partly covered with graphene, resulting in only a small reduction of e-beam damage. But, the clear damage reduction observed for Li_2O_2 encapsulated in a graphene cell suggests that even partial graphene coverage can delay the decomposition of Li_2O_2. Although the exact mechanisms responsible for the reduction of beam damage are difficult to determine with certainty, the remarkable electric and thermal conduction of graphene is expected to contribute effectively to dissipating accumulated charge and/or heat under an electron beam. However, comparing results from different parts of a graphene cell, we found that the effectiveness of graphene cell is not consistent throughout the grid. This is probably due to the flawed attachment of graphene sheets and Li_2O_2 particles at that particular area. Functionalization of graphene sheets may improve the attachment properties.

Note that, for both standard grid and graphene cells, lower electron dose rates delay the decomposition onset. However, at higher dose rates, decomposition onset does not appear to occur at all (Fig. 7(b)). This suggests the possibility of a threshold dose rate below which an onset of decomposition can be found. However, by comparing the total dose required for a 50% Li_2O_2 decomposition (Fig. 8) in a standard grid and a graphene cell at different dose rates, we found that the total dose required for decomposition is roughly independent of the e-beam dose rate. This implies that decomposition is dependent on the total dose.

We found that Li_2O_2 could withstand STEM scanning for 30 min for electron dose rates lower than 100 e/nm^{2}s without decomposing at all. Therefore, one may conclude that Li_2O_2 can withstand a higher electron dose in STEM mode than in TEM mode. However, when we calculate the total dose to which Li_2O_2 particles were exposed during STEM scanning, we found it to be one order of magnitude less than that required to decompose Li_2O_2 particles in TEM mode [Table S-8]. Furthermore, as mentioned above, increasing the dose rate by decreasing the pixel size (*i.e.*, increasing the magnification) and/or increasing the beam dwell time accelerates the decomposition of Li_2O_2. Although this result suggests at first glance that the decomposition is dose rate dependent, our calculations of

the total dose clearly shows that decomposition is dependent on the total electron dose [Table S-8].

5. Conclusion

TEM provides the ability to obtain chemical, structural and morphological information about discharge products at a local scale, which is essential for understanding the complex chemistry and further improving Li–O_2 battery technology. However, we have shown how the sensitivity of discharge products to air exposure and electron-beam irradiation limits the application of TEM in Li–O_2 battery research.

Concerning damage caused by e-beam irradiation, we found that the onset of Li_2O_2 decomposition occurs 4 to 5 times faster at 80 than at 200 kV electrons for the same dose rate. Therefore, we recommend that relatively high acceleration voltages be used in TEM studies. However, for acquiring chemical information using EEL spectra, one should bear in mind that the EELS signal also increases at low acceleration voltages, therefore the signal/damage ratio is independent of accelerating voltages without considering signal-collection efficiency and statistical noise [11].

As decomposition is dependent on the total dose, using a low e-beam dose rate obviously delays the onset of decomposition and thereby allows the sample to be analysed in its pristine state. For instance, at 200 kV in TEM mode, the onset of Li_2O_2 decomposition occurs after 60 s at an electron dose rate of 1900 e/nm^{2}s compared to 20 s at 8900 e/nm^{2}s. The total dose rate-dependent decomposition is also evident in STEM mode, where no decomposition of Li_2O_2 is evident until a total dose of 4.8×10^4 e/nm^2 has been reached.

We also found it necessary to avoid air contact to preserve the sample in its pristine state. This can be achieved by using a TEM holder with vacuum transfer functionality or a “graphene cell”, where the discharge product is encapsulated between two graphene sheets that protect the sample from air contact while being transferred to the TEM.

A graphene cell also delays the onset of e-beam degradation compared to the sample on a standard TEM grid. Although the performance of the graphene cell is not consistent throughout the grid, probably due to faulty encapsulation, and further work is needed to improve the contact between the graphene and the Li_2O_2 or other beam-sensitive materials, we can nevertheless conclude that graphene cells are promising carriers for studying Li–O_2 battery discharge products.

Acknowledgements

Authors like to thank Dr. Qian Chen for sharing the knowledge of preparing graphene grids; Dr. Swapna Ganapathy and Dr. Marnix Wagemaker for providing and the samples. This work was financially supported by NWO NANO project 11498 and ERC project 267922.

Conflicts of interest

None.

Supplementary materials

Supplementary material associated with this article can be found, in the online version, at doi:10.1016/j.ultramic.2018.03.005.

References

[1] B.D. Adams, R. Black, C. Radtke, Z. Williams, B.L. Mehdi, N.D. Browning, L.F. Nazar, The importance of nanometric passivating films on cathodes for Li-Air batteries, ACS Nano 8 (12) (2014) 12483–12493. https://doi.org/10.1021/nn505337p.

[2] G. Algara-Siller, S. Kurasch, M. Sedighi, O. Lehtinen, U. Kaiser, The pristine atomic structure of MoS2 monolayer protected from electron radiation damage by graphene, Appl. Phys. Lett. 103 (20) (2013). https://doi.org/10.1063/1.4830036.

[3] M. Balaish, A. Kraytsberg, Y. Ein-Eli, A critical review on lithium-air battery electrolytes, Phys. Chem. Chem. Phys. 16 (7) (2014) 2801–2822. https://doi.org/10.1039/C3CP54165G.

[4] D. Capsoni, M. Bini, S. Ferrari, E. Quartarone, P. Mustarelli, Recent advances in the development of Li-air batteries, J. Power Sources 220 (2012) 253–263. https://doi.org/10.1016/j.jpowsour.2012.07.123.

[5] Y. Chang, S. Dong, Y. Ju, D. Xiao, X. Zhou, L. Zhang, G. Cui, A carbon- and binder-free nanostructured cathode for high-performance nonaqueous Li-O_2 battery, Adv. Sci. (2015). n/a-n/a https://doi.org/10.1002/advs.201500092.

[6] Q. Chen, J.M. Smith, J. Park, K. Kim, D. Ho, H.I. Rasool, A.P. Alivisatos, 3D motion of DNA-Au nanoconjugates in graphene liquid cell electron microscopy, Nano Lett. 13 (9) (2013) 4556–4561. https://doi.org/10.1021/nl402694n.

[7] J. Christensen, P. Albertus, R.S. Sanchez-Carrera, T. Lohmann, B. Kozinsky, R. Liedtke, A. Kojic, A critical review of Li/Air batteries, J. Electrochem. Soc. 159 (2) (2012) R1. https://doi.org/10.1149/2.086202jes.

[8] R.F. Egerton, Electron energy-loss spectroscopy in the TEM, Rep. Prog. Phys. 72 (1) (2008) 16502. https://doi.org/10.1088/0034-4885/72/1/016502.

[9] R.F. Egerton, Mechanisms of radiation damage in beam-sensitive specimens, for TEM accelerating voltages between 10 and 300kV, Microsc. Res. Tech. 75 (11) (2012) 1550–1556. https://doi.org/10.1002/jemt.22099.

[10] R.F. Egerton, Control of radiation damage in the TEM, Ultramicroscopy 127 (2013) 100–108.

[11] R.F. Egerton, P. Li, M. Malac, Radiation damage in the TEM and SEM, Micron 35 (6) (2004) 399–409. https://doi.org/10.1016/j.micron.2004.02.003.

[12] N. Feng, P. He, H. Zhou, Critical challenges in rechargeable aprotic Li-O2 batteries, Adv. Energy Mater. 6 (9) (2016) 1–24. https://doi.org/10.1002/aenm.201502303.

[13] S.A. Freunberger, Y. Chen, Z. Peng, J.M. Griffin, L.J. Hardwick, F. Bardé, P.G. Bruce, Reactions in the rechargeable lithium-O2 battery with alkyl carbonate electrolytes, J. Am. Chem. Soc. 133 (20) (2011) 8040–8047. https://doi.org/10.1021/ja2021747.

[14] H. Geaney, C. O'Dwyer, Examining the role of electrolyte and binders in determining discharge product morphology and cycling performance of carbon cathodes in Li-O-2 batteries, J. Electrochem. Soc. 163 (2) (2016) A43–A49. https://doi.org/10.1149/2.1011514jes.

[15] G. Girishkumar, B. McCloskey, A.C. Luntz, S. Swanson, W. Wilcke, Lithium-air battery: promise and challenges, J. Phys. Chem. Lett. 1 (14) (2010) 2193–2203. https://doi.org/10.1021/jz1005384.

[16] Y. Hu, X. Han, F. Cheng, Q. Zhao, Z. Hu, J. Chen, Size effect of lithium peroxide on charging performance of Li-O2 batteries, Nanoscale 6 (1) (2014) 177–180. https://doi.org/10.1039/c3nr04728h.

[17] S. Lau, L.A. Archer, Nucleation and growth of lithium peroxide in the Li-O<inf>2</inf>battery, Nano Lett. 15 (9) (2015) 5995–6002. https://doi.org/10.1021/acs.nanolett.5b02149.

[18] F. Li, D.M. Tang, Y. Chen, D. Golberg, H. Kitaura, T. Zhang, H. Zhou, Ru/ITO: a carbon-free cathode for nonaqueous Li-O2 battery, Nano Lett. 13 (10) (2013) 4702–4707. https://doi.org/10.1021/nl402213h.

[19] Y.-C. Lu, B.M. Gallant, D.G. Kwabi, J.R. Harding, R.R. Mitchell, M.S. Whittingham, Y. Shao-Horn, Lithium–oxygen batteries: bridging mechanistic understanding and battery performance, Energy Environ. Sci. 6 (3) (2013) 750. https://doi.org/10.1039/c3ee23966g.

[20] B.D. McCloskey, A. Speidel, R. Scheffler, D.C. Miller, V. Viswanathan, J.S. Hummelshøj, A.C. Luntz, Twin problems of interfacial carbonate formation in nonaqueous Li-O2 batteries, J. Phys. Chem. Lett. 3 (8) (2012) 997–1001. https://doi.org/10.1021/jz300243r.

[21] M. M., Ottakam Thotiyl, S.A. Freunberger, Z. Peng, Y. Chen, Z. Liu, P.G. Bruce, A stable cathode for the aprotic Li-O2 battery, Nat. Mater. 12 (11) (2013) 1050–1056. https://doi.org/10.1038/nmat3737.

[22] M.M. Ottakam Thotiyl, S.A Freunberger, Z. Peng, Y. Chen, Z. Liu, P.G. Bruce, A stable cathode for the aprotic Li-O2 battery, Nat. Mater. 12 (2013) 1050–1056. (September) https://doi.org/10.1038/nmat3737 .

[23] Z. Peng, S.A. Freunberger, Y. Chen, P.G. Bruce, A reversible and higher-rate Li-O2 battery, Science 337 (6094) (2012) 563–566. https://doi.org/10.1126/science.1223985.

[24] R. Qiao, Y.De Chuang, S. Yan, W. Yang, Soft x-ray irradiation effects of Li2O2, Li2CO3 and Li2O revealed by absorption spectroscopy, PLoS ONE 7 (11) (2012) 3–8. https://doi.org/10.1371/journal.pone.0049182.

[25] M.A. Rahman, X. Wang, C. Wen, A review of high energy density lithium-air battery technology, J. Appl. Electrochem. 44 (1) (2014) 5–22. https://doi.org/10.1007/s10800-013-0620-8.

[26] A.B. Tsentsiper, Z.I. Kuznetsova, Thermal decomposition of lithium peroxide, Bull. Acad. Sci. USSR Div. Chem. Sci. 14 (10) (1965) 1873–1875. https://doi.org/10.1007/BF00850186.

[27] K.P.C. Yao, D.G. Kwabi, R.A. Quinlan, A.N. Mansour, A. Grimaud, Y.-L. Lee, Y. Shao-Horn, Thermal stability of Li2O2 and Li2O for Li-air batteries: in situ XRD and XPS studies, J. Electrochem. Soc. 160 (6) (2013) A824–A831. https://doi.org/10.1149/2.069306jes.

[28] R. Zan, Q.M. Ramasse, R. Jalil, T. Georgiou, U. Bangert, K.S. Novoselov, Control of radiation damage in MoS2 by graphene encapsulation, ACS Nano 7 (11) (2013) 10167–10174. https://doi.org/10.1021/nn4044035.